Loss of polarization of elliptically polarized collapsing beams

Gauri Patwardhan,[1,2,*] Xiaohui Gao,[1] Amir Sagiv,[3] Avik Dutt,[4,5] Jared Ginsberg,[1] Adi Ditkowski,[3] Gadi Fibich,[3] and Alexander L. Gaeta[1,†]

[1]*Department of Applied Physics and Applied Mathematics, Columbia University, New York, New York 10027, USA*
[2]*School of Applied and Engineering Physics, Cornell University, Ithaca, New York 14853, USA*
[3]*Department of Applied Mathematics, Tel Aviv University, Tel Aviv 6997801, Israel*
[4]*Department of Electrical Engineering, Columbia University, New York, New York 10027, USA*
[5]*School of Electrical and Computer Engineering, Cornell University, Ithaca, New York 14853, USA*

(Received 3 August 2018; published 12 March 2019)

We show theoretically and demonstrate experimentally that collapsing elliptically polarized laser beams experience a nonlinear ellipse rotation that is highly sensitive to small fluctuations in the input power. For arbitrarily small fluctuations in the input power and after a sufficiently large propagation distance, the polarization angle becomes uniformly distributed in $[0, 2\pi]$ from shot to shot. We term this phenomenon loss of polarization. We perform experiments in fused-silica glass, nitrogen gas, and water and observe a significant increase in the fluctuations of the output polarization angle for elliptically polarized femtosecond pulses as the power is increased beyond the critical power for self-focusing. We also show numerically and confirm experimentally that this effect is more prominent in the anomalous group-velocity dispersion (GVD) regime compared to the normal-GVD regime due to the extended lengths of the filaments for the former. Such effects could play an important role in intense-field light-matter interactions in which elliptically polarized pulses are utilized.

DOI: 10.1103/PhysRevA.99.033824

I. INTRODUCTION

Optical beam collapse occurs when a laser beam with a power greater than a certain critical power P_{cr} propagates through a transparent medium and undergoes self-focusing [1–5]. At higher powers, competing effects such as plasma defocusing arrest the collapse, leading to the formation of laser filaments [6–8] that can confine light over distances much longer than the diffraction length [9]. Self-focusing and laser filamentation are important for applications in atmospheric remote sensing [10,11], light detection and ranging [9,12], high-harmonic generation (HHG) [13–15], pulse compression [12], and terahertz generation [16]. Additionally, collapsing waves are of universal interest because of their relevance not only in optics but also in a wide variety of fields, e.g., in Bose-Einstein condensation, surface waves dynamics, plasma physics, and Ginzburg-Landau equations [17–20].

Through the process of self-phase modulation, the acquired nonlinear phase shift of collapsing beams becomes large and highly sensitive to small fluctuations in the input power, as predicted theoretically [21,22] and demonstrated experimentally [23]. Furthermore, as the collapsing beam evolves into a filament, the sensitivity of the nonlinear phase shift to small fluctuations increases with the propagation distance, so that ultimately, the nonlinear phase shift becomes uniformly distributed in $[0,2\pi]$ [24]. As a result of this loss of phase, the interference between postcollapse beams becomes chaotic [22–26].

While the effects of beam collapse on the electric-field amplitude and phase have been extensively investigated [22,23,27–30], limited work exists on the study of the polarization of beams undergoing wave collapse. Most of the work studies the effects of polarization on beam collapse [31–37]. However, the change in the beam's polarization itself as a result of its collapse remains largely unexplored. Since several applications of laser filamentation including HHG, THz generation, and supercontinuum generation are polarization sensitive [38–40], investigating the polarization state of collapsing beams is crucial [41–43]. In some of the studies, molecular alignment and delayed birefringence acting on the probe were investigated [44–46]. In the case of self-induced polarization rotation of the pump, direct measurements [47] using a rotating polarizing cube and indirect measurements [48] using femtosecond laser-induced periodic surface structures have observed moderate rotations of the polarization angle pre- and postcollapse. The fluctuations in polarization rotation in these studies, however, were obscured by averaging over multiple shots or pulse periods, and the increase of the fluctuations with propagation distance at powers significantly above P_{cr} was not revealed. Additionally, theoretical investigations based on these observations have not been performed.

In this paper, we theoretically predict and experimentally demonstrate an effect which we term loss of polarization. We show that, when an elliptically polarized input beam undergoes filamentation, its nonlinear ellipse rotation can become highly sensitive to fluctuations in the input power. Hence, its output polarization becomes random. We show the

*gnp22@cornell.edu
†a.gaeta@columbia.edu

universality of the loss of polarization effect by performing experiments with femtosecond pulses in various media (glass, water, and nitrogen gas). For glass we perform experiments under conditions of normal and anomalous group-velocity-dispersion (GVD) and show that the loss-of-polarization effect is more pronounced in the anomalous-GVD regime where filaments tend to be significantly longer.

II. THEORY AND SIMULATIONS

To theoretically explain the loss of polarization in elliptically polarized, collapsing beams, we consider the nonlinear Schrödinger equations (NLSEs) for propagation in a bulk saturable Kerr medium

$$\frac{\partial A_\pm}{\partial z} = i\left\{\frac{\partial^2 A_\pm}{\partial x^2} + \frac{\partial^2 A_\pm}{\partial y^2} + \frac{2}{3}\frac{(|A_\pm|^2 + 2|A_\mp|^2)A_\pm}{[1+\epsilon(|A_\pm|^2+|A_\mp|^2)]}\right\}, \tag{1}$$

where $A_+(z,x,y)$ and $A_-(z,x,y)$ are the slowly varying envelopes of the clockwise and counterclockwise circular polarization components of the electric field, respectively, x and y are the transverse coordinates normalized by the input beam radius, z is the coordinate along the propagation direction normalized by the diffraction length, and ϵ is the saturation parameter. The angle θ between the major axis of the polarization ellipse and the x axis is [48]

$$\theta(z) = -\frac{1}{2}\tan^{-1}\frac{U}{Q}, \tag{2}$$

where $U = -2\ \mathrm{Im}[\int A_+^* A_-\, dx\, dy]$ and $Q = 2\ \mathrm{Re}[\int A_+^* A_-\, dx\, dy]$.

An elliptically polarized Gaussian input beam, whose power P_{in} is moderately above P_{cr}, evolves into the coupled spatial solitary waves

$$A_\pm(z,x,y) = e^{i\kappa_\pm Z} R_\pm(x,y), \tag{3}$$

where $R_\pm$ are solutions of

$$-\kappa_\pm R_\pm + \frac{\partial^2 R_\pm}{\partial x^2} + \frac{\partial^2 R_\pm}{\partial y^2} + \frac{2}{3}\frac{(|R_\pm|^2 + 2|R_\mp|^2)R_\pm}{[1+\epsilon(|R_\pm|^2+|R_\mp|^2)]} = 0.$$

When the Gaussian input beam is elliptically polarized, the power of $A_+(0,x,y)$ is different from that of $A_-(0,x,y)$. Hence, A_+ and A_- converge to different solitary waves with $\Delta\kappa = \kappa_+ - \kappa_- \neq 0$, and the beam accumulates a polarization angle θ_0 during the initial collapse stage. The polarization rotation angle then satisfies (see Appendix A)

$$\theta(z) = \theta_0 + \frac{\Delta\kappa}{2}z. \tag{4}$$

In the presence of input noise, θ_0 and $\Delta\kappa$ become random variables, therefore, by the loss of phase lemma [24], the probability distribution of θ mod (2π) converges to a uniform distribution on $[0, 2\pi]$ as $z \to \infty$. This effect represents a complete *loss of polarization*. For z sufficiently large so that $z\Delta P\,(d\Delta\kappa/dz) \gg 1$, even for small changes in the input power ΔP, large changes in θ are induced, making it impossible to deterministically predict the output polarization angle. Note that, for a linearly polarized input beam, since $|A_+| = |A_-|$, both components collapse into identical solitary waves with $\Delta\kappa = 0$, and so the polarization angle does not rotate at all. Additionally, in the case of purely circular polarization, only one of A_+ or A_- is present [see Eq. (1)], and ellipse rotation in this case does not have meaning, and the beam remains circularly polarized.

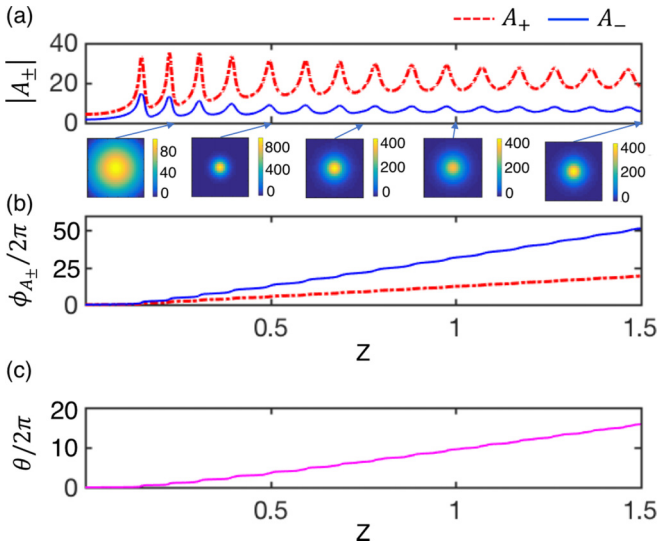

FIG. 1. Solution of Eq. (1) assuming a Gaussian initial beam profile with $P_{in}/P_{cr} = 1.73$. (a) On-axis amplitude $|A(z,0)|$ and beam profile vs propagation distance z; (b) unwrapped on-axis phase ϕ for right (left) circularly polarized component indicated by the red-dotted (blue-solid) curve; (c) the polarization angle $\theta(z)$ vs z.

To demonstrate the loss of polarization phenomenon numerically, we solve the coupled NLSE [Eq. (1)] using the split-step Fourier transform method [49] with $\epsilon = 5\times10^{-5}$ and $|A_+/A_-|_{z=0} = 2.747$. Both components collapse and evolve into solitary waves; see Fig. 1(a). The bottom plots of Fig. 1(a) show the spatial intensity profile of the beam at various propagation lengths. The difference in amplitude between the two components in Fig. 1(a) corresponds to a difference in their propagation constants; see Eq. (3). This is shown by the different slopes of the on-axis accumulated phases in Fig. 1(b) ($\kappa_- \approx 75.82$ and $\kappa_+ \approx 26.49$). Since $\Delta\kappa \approx 49.33$, theoretical prediction of the polarization angle $\theta(z) \approx z\Delta\kappa(P)/2 \approx 24.66z$ by Eq. (4) agrees well with the direct fit of $\theta(z) \approx 24.47z$ [Eq. (2)] in Fig. 1(c), whose slope is within 0.8% of the theoretical prediction. To the best of our knowledge, Fig. 1 presents the first example of a multicomponent solitary wave of the NLSE with different propagation constants for each component.

Figure 2 shows the polarization angle θ as a function of the input power, for various propagation distances z. The elliptically polarized beam undergoes negligible change in the accumulated polarization angle for short propagation lengths ($z = 0.1$) [Fig. 2(a)], so the probability distribution function (PDF) is highly localized [Fig. 2(d)]. As the propagation distance increases ($z = 0.5$), these changes increase [Fig. 2(b)], and the PDF becomes more spread out, i.e., the uncertainty in θ increases [Fig. 2(e)]. Ultimately, at long propagation lengths ($z = 1.5$), θ varies rapidly with the power [Fig. 2(c)], and the PDF approaches a uniform distribution [Fig. 2(f)]. The PDFs in Figs. 2(d)–2(f) were computed using a numerical method which is more efficient and informative for a fixed number

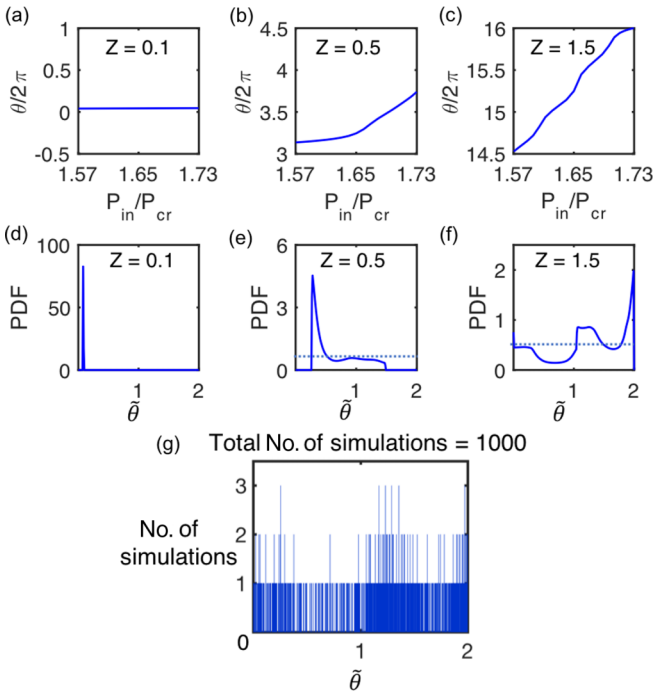

FIG. 2. Elliptically polarized input beam. (a)–(c) Polarization angle vs input power at $z = 0.1$, 0.5, and 1.5, respectively; (d)–(f) the probability distribution function (PDF) of $\tilde{\theta} = \theta/\pi (\text{mod } 2)$; at $z = 0.1$, 0.5, and 1.5; (g) histogram of $\tilde{\theta}$ at $z = 1.5$ for 1000 simulations with P_{in}/P_{cr} distributed uniformly in [1.53, 1.75].

of NLSE simulations than the Monte Carlo method [50]. We illustrate the loss of polarization at $z = 1.5$ by plotting a histogram of 1000 simulations with an elliptically polarized input beam with P_{in} distributed uniformly in the 10% interval around $1.65P_{cr}$ and observe that θ fluctuates across the entire range of $[0,2\pi]$ [Fig. 2(g)].

As predicted by theory, linearly polarized beams do not undergo loss of polarization. Indeed, our simulations show that the polarization angle of a linearly polarized beam remains unchanged irrespective of P_{in} (simulation results are presented in Fig. 5 in Appendix B).

III. EXPERIMENTS

We experimentally investigate the stability of the output polarization after the beam has undergone collapse for different input polarizations (linear and elliptical) in fused silica. We loosely focus pulses from an optical parametric amplifier (OPA) (HE-TOPAS-prime, Light Conversion, Inc.) at a wavelength of 1550 nm (75-fs pulse duration, 10-Hz repetition rate) into a 5-cm-long glass sample using a 50-cm focal length lens. The OPA is pumped by a Coherent HIDRA amplifier with 800-nm, 50-fs, 10-Hz pulses. We control the input light polarization with the help of a quarter-wave plate (QWP) and a half-wave plate (HWP). The input light undergoes collapse inside the glass sample and is collimated by a lens at the output. We separate the s- and p-polarization components with a Glan prism and monitor their energy on two InGaAs detectors. The experimental setup is shown in Fig. 3(a). The energy of the input pulses is varied from 15 to 220 μJ.

In each single-shot measurement, the recorded magnitudes of the s and p polarizations (P_{0y} and P_{0x}) are proportional to the square of the electric field amplitude for the y and x component, respectively. θ can be explicitly calculated from these values using the following equation [51]:

$$\tan(2\theta) = \frac{2\sqrt{P_{0x}}\sqrt{P_{0y}}\cos(\delta)}{(P_{0x} - P_{0y})}, \tag{5}$$

where δ is the phase offset between the x and y components of the electric field, i.e., $\delta = 0$ represents linear polarization and $\delta = \pi/2$ with $E_{0x} = E_{0y}$ represents circular polarization. The ellipticity of the elliptically polarized input used in our experiment is 0.447, corresponding to a δ of 67.4° and $\cos(\delta) = 0.384$. Beam collapse is indicated by the presence of white light at the output due to the generated supercontinuum as a result of filamentation and glass ionization [3,52–54]. It also indicates in the plotted curve output energy in p polarization ("p-pol") versus input energy [Fig. 3(b)]. When the input energy is low, the output energy varies linearly with input as expected. When collapse occurs, the transmitted energy saturates due to nonlinear absorption inside the glass sample, and the slope of the output energy versus input energy decreases as shown in Fig. 3(b). Input energies are normalized to the maximum energy used in our experiments (220 μJ). From both indicators, we determine that the beam collapse begins at around 0.25 of the normalized energy. We plot normalized energies in the s versus p polarization in Fig. 3(c) to show trends in θ. For linearly polarized input, irrespective of whether collapse and filamentation occur, the curve of s- versus p-polarized energy is linear, indicating a constant polarization angle. For elliptically polarized input, in the absence of beam collapse at low powers, the s versus p plot shows a $\tan^2$ dependence that arises due to steady increase of θ with power, in agreement with the theory (see Appendix C). At high energies, however, s versus p exhibits random behavior due to loss of polarization. To further investigate this effect, the s/p fluence ratio is calculated from each single-shot measurement by taking the ratio of the corresponding detector outputs and is plotted as a function of input energy for elliptically and linearly polarized light [Fig. 3(d)]. The fluctuations in the s/p fluence ratio are correlated to the fluctuations in θ. The resulting plot shows two important features. First, for elliptically polarized input, the s/p ratio steadily increases with input energy, showing a rotation of the polarization ellipse, whereas for linear input the s/p ratio stays constant, indicating a constant polarization angle. Second, the fluctuations in the s/p ratio increase for elliptically polarized input, indicating increased sensitivity of the output polarization angle on input power. For the case of linearly polarized input, fluctuations in s/p ratio remain small and constant throughout. These observations are in accordance with our theoretical prediction based on the nonlinear ellipse rotation phenomenon [55]. Below the collapse threshold ($<$55 μJ or 0.25 of normalized input energy), the fluctuations for the elliptically polarized beam are comparable to the small fluctuations ($\sim$1°) for the linearly polarized beam. However, for sufficiently high input energy ($>$55 μJ), i.e., when the beam undergoes collapse, the fluctuations become six times higher for elliptically polarized input than for linearly polarized input, which agrees

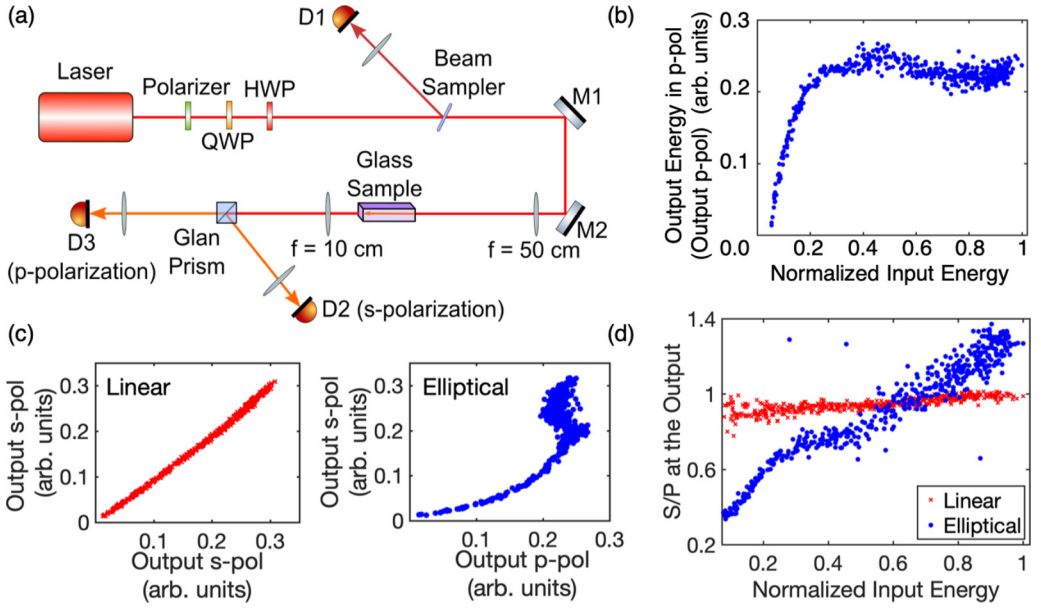

FIG. 3. (a) Experimental setup. QWP: quarter wave plate, HWP: half wave plate, D1, D2, D3: InGaAs detectors. (b) Energy in the output p polarization vs normalized input energy for an elliptically polarized beam. We obtain a similar graph for energy in the output s polarization. (c) Output s polarization vs p polarization for linearly (red, left) and elliptically (blue, right) polarized input. (d) Plot of s/p ratio vs input energy for linearly (red crosses) and elliptically (blue circles) polarized input.

qualitatively with our numerical predictions. We observe a 27° rotation of polarization angle over the entire energy interval in our experiment for elliptically polarized input. The observed fluctuations in the polarization angle are more than 6° for the highest energy in our experiment. This is significantly larger than the measurement uncertainty (1°), which we calculate based on the fluctuations in θ in the linear-polarization case.

IV. EFFECT OF DISPERSION

From our analysis [see Eq. (4)] and the NLSE simulations (Fig. 1), we predict that as the propagation distance increases, the sensitivity of the output polarization angle to the input power fluctuations increases. Researchers have previously shown that filaments in the anomalous group-velocity dispersion (GVD) regime are longer and more stable and yield more collapsing events as compared to those in the normal-GVD regime [56–59]. Thus, we expect that the loss of polarization effect would be more prominent in the anomalous-GVD regime. To test this hypothesis, we performed simulations including effects of dispersion, diffraction, and nonlinearity for a material with GVD ($\beta_2 = \pm 26$ ps^2/km) similar to glass, 75-fs pulse duration, and input power uniformly distributed between $17.4P_{cr}$ and $19.2P_{cr}$ (further details are given in Appendix D). The s/p ratio was calculated using the output polarization angle at $z = 0.05$. Our simulation results are shown in Figures 4(a) and 4(b). For consistency with simulations in the anomalous-GVD regime ($\beta_2 = -26$ ps^2/km), we use ($\beta_2 = +26$ ps^2/km) in the normal-GVD-regime simulations. However, our normal-GVD regime experiments were performed with a laser at 800 nm, where β_2 for glass is slightly different (+35 ps^2/km). In the normal-GVD regime, calculated shot-to-shot fluctuations (indicated by the light-blue-shaded region in the plots) in the output polarization angle were 4.9°, whereas those in the anomalous-GVD regime were about 7.8° (1.6 times larger). We also performed corresponding experiments in glass with pulses at 800 nm (normal-GVD regime, $\beta_2 = +35$ ps^2/km) and at 1500 nm (anomalous-

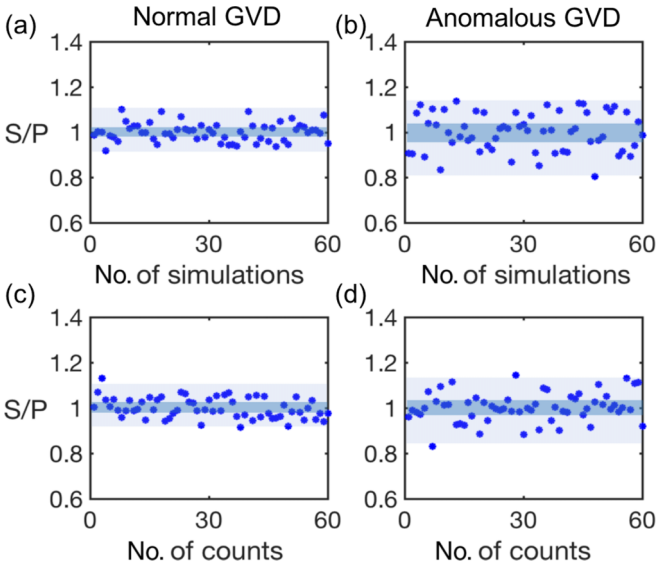

FIG. 4. s/p fluence ratios at the output for elliptically polarized input. Variance (σ) shown by dark blue shaded region, shot-to-shot fluctuations shown by light-blue-shaded region. (a), (b) Simulation results with input power varied uniformly between $17.4P_{cr}$ and $19.2P_{cr}$l (c), (d) experimental results in glass at 800 nm and 1500 nm, respectively, input energy varied 10% around (c) 88 μJ and (d) 176 μJ. Experimental results follow the simulation trend that fluctuations are more pronounced in the anomalous-GVD [$\sigma = 0.084$ (simulation), 0.063 (experiment)] than those in the normal-GVD regime [$\sigma = 0.041$(simulation), 0.045(experiment)].

GVD regime, $\beta_2 = -26\ \mathrm{ps}^2/\mathrm{km}$). Figures 4(c) and 4(d) show our experimental results for the normal and anomalous-GVD regime, respectively. Measured shot-to-shot fluctuations in the output polarization angle for the normal-GVD regime were 4.3°, whereas those in the anomalous-GVD regime were 6° (1.4 times larger). Experimental results follow the trend predicted in simulations and confirm our hypothesis that the output polarization angle is more sensitive to the input power in the anomalous-GVD regime than in the normal-GVD regime. In all the plots in Fig. 4, the input power (energy) is varied by 10% [±5%].

V. UNIVERSALITY

This increase in fluctuations occurs in all media whenever there is filamentation of elliptically polarized beams. To demonstrate this, we performed experiments in glass, liquid water, and nitrogen gas at 23-bar pressure, using 800-nm, 50-fs pulses at a 10-Hz repetition rate (normal-GVD regime). In all these cases, we compare output s/p ratio fluctuations for elliptically polarized input and linearly polarized input for fixed 10% fluctuations in input energy. We observed that at low pulse energies (below the collapse threshold), the fluctuations in s/p ratio for both input polarizations are identical. On the other hand, above the collapse threshold, fluctuations in s/p ratio in the case of elliptically polarized input are two to four times higher than the fluctuations in case of linearly polarized input. This indicates that θ is more sensitive to input power fluctuations for elliptically polarized light as compared to linearly polarized light, in agreement with the loss of polarization theory. (Plots are presented in Figs. 6, 7, and 8 in Appendix E).

VI. SUMMARY AND OUTLOOK

In conclusion, we theoretically show that the loss of polarization angle increases with propagation distance and ultimately leads to a complete loss of polarization angle for collapsing beams of elliptical polarization. We provide experimental evidence for this effect by measuring a significant increase in the fluctuations of the polarization angle in a glass sample. We demonstrate that the loss of polarization effect is more prominent in the anomalous-GVD regime. Such behavior is universal and should occur in all systems that exhibit multiple collapse of elliptically polarized beams. Furthermore, this work can be extended to study beam polarization for multifilamentation. In this case, the loss of the polarization effect could lead to spatial depolarization of the beam due to unequal polarization rotation in each filament. Recent work shows that light with different spatial profiles such as vortex Airy beams and axially asymmetric beams have controllable and designable collapse dynamics that are robust against random noise [60–63], and it is expected that the loss-of-polarization effect could also occur in such beams. Our work has implications for applications that depend upon the beam polarization being deterministic for collapsing beams traveling over long distances, such as in filamentation for remote sensing and HHG.

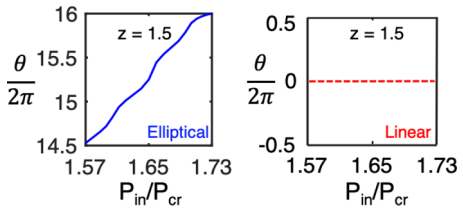

FIG. 5. Simulation results for polarization angle as a function of input power ($\theta/2\pi$ vs P_{in}/P_{cr}) at $z = 1.5$ for linear (elliptical) input polarization shown by red dashed (blue solid) line in the right (left) plot.

ACKNOWLEDGMENTS

The research of G.P., X.G., J.G., and A.L.G. was supported by the Air Force Office of Scientific Research (AFOSR) Multidisciplinary University Research Initiative under Award No. FA9550-16-1-0121. The research of A.S. and G.F. was partially supported by Grant No. 177/13 from the Israel Science Foundation (ISF).

APPENDIX A: DERIVATION OF EQ. (4)

Substituting (3) into (2) yields

$$U = -2\mathrm{Im}\left[\int A_+^* A_- \, dx\, dx\right] = 2\sin(z\kappa_+ - z\kappa_-)\int R_+ R_- \, dx\, dy$$

and

$$Q = 2\mathrm{Re}\left[\int A_+^* A_- \, dx\, dx\right] = 2\cos(z\kappa_+ - z\kappa_-)\int R_+ R_- \, dx\, dy.$$

Therefore, denoting $\Delta\kappa = \kappa_+ - \kappa_-$, we have by (2),

$$\theta(z) = -\frac{1}{2}\tan^{-1}\frac{U}{Q} = -\tan^{-1}[\tan(z\Delta\kappa)] = \frac{\Delta\kappa}{2}z.$$

Finally, adding θ_0, the polarization rotation angle accumulated during the initial collapse stage, yields (3).

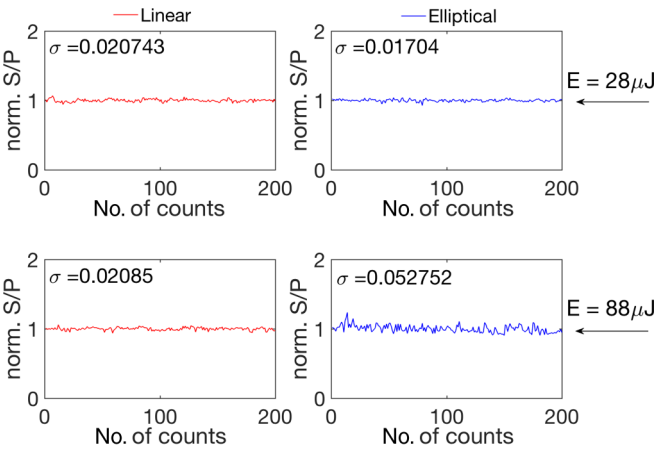

FIG. 6. Results in glass for fluctuations in a normalized s/p ratio over 200 consecutive shots.

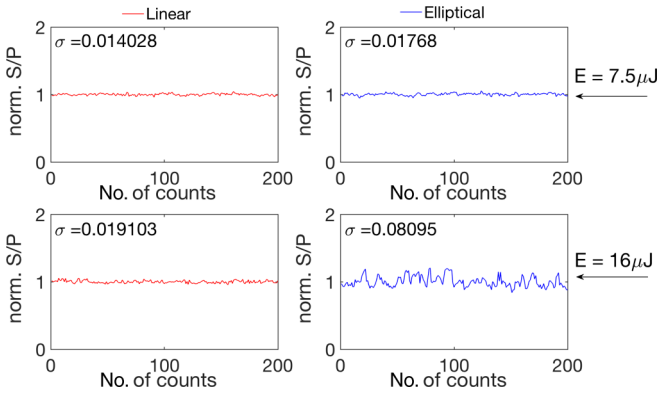

FIG. 7. Results in water for fluctuations in a normalized s/p ratio over 200 consecutive shots.

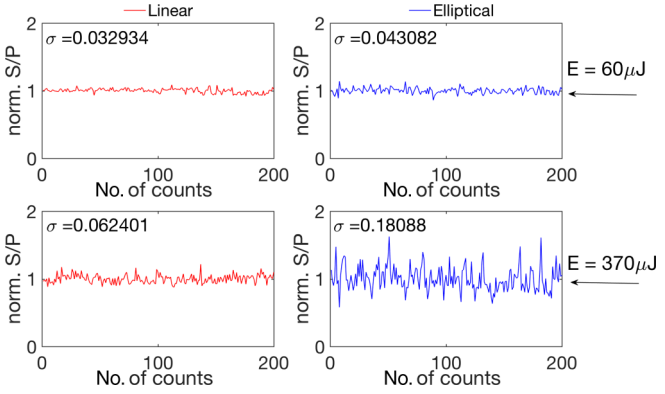

FIG. 8. Results in high-pressure nitrogen gas for fluctuations in a normalized s/p ratio over 200 consecutive shots.

APPENDIX B: POLARIZATION ANGLE θ VERSUS INPUT POWER FOR LINEAR POLARIZATION

Simulation results for polarization angle as a function of input power at $z = 1.5$ for linear (right side plot) and elliptical (left side plot) input polarization are shown in Fig. 5. Note that the left plot is the Fig. 2(c) elliptical input case shown for comparison with the linear input case.

The polarization angle for elliptically polarized input varies by more than 2π when the input power is changed in the 10% interval around $1.65P_{cr}$, whereas the polarization angle for linearly polarized input remains unchanged for the same variation in input power.

APPENDIX C: EXPLANATION OF STEADY INCREASE OF θ WITH POWER FOR ELLIPTICAL POLARIZATION

The polarization angle θ due to nonlinear ellipse rotation can be given by [55] $\theta = \frac{1}{2}\Delta n \frac{\omega}{c} z$, where $\Delta n \equiv \frac{B}{2n_0}(|A_-|^2 - |A_+|^2)$. Here B is a material-dependent constant and n_0 is the refractive index. For a given ellipticity, in the linear propagation regime, $|A_-|^2 \propto$ input power (P_{in}) and $|A_-|^2 \propto P_{in}$, so, $\Delta n \propto P_{in}$. Thus, assuming negligible losses, $\theta \propto P_{in}$.

At powers below critical power P_{cr}, the propagation of light in the medium is linear, and the losses are low. Therefore at these conditions, θ increases with the input power, leading to steady increase of the s/p ratio as shown in Fig. 3(d) for elliptical polarization.

Output s polarization is correlated to $\sin^2(\theta)$, and p polarization is correlated to $\cos^2(\theta)$. Therefore, with steadily increasing θ, the plot of s polarization versus p polarization in Fig. 3(c) shows a quadratic looking $\tan^2$ dependence for elliptical polarization, at low input energies.

APPENDIX D: DETAILS OF SIMULATIONS WITH DISPERSION

The simulations to study the effects of anomalous versus normal GVD were carried out using a modified form of Eq. (1) including effects of group-velocity dispersion:

$$\frac{\partial A_\pm}{\partial z} = i\left\{\frac{\partial^2 A_\pm}{\partial x^2} + \frac{\partial^2 A_\pm}{\partial y^2} - \frac{\beta_2}{2}\frac{\partial^2 A_\pm}{\partial t^2} + \frac{2}{3}\frac{(|A_\pm|^2 + 2|A_\mp|^2)A_\pm}{[1+\epsilon(|A_\pm|^2 + |A_\mp|^2)]}\right\}.$$

Since our pulses have a moderate spectral bandwidth, the effects of higher-order dispersion and self-steepening can be neglected. Additionally, it was shown by Shim *et al.* [23] that the loss of phase effect occurs for a wide variety of nonlinear saturation terms, including higher-order Kerr nonlinearities and plasma defocusing. Similar conclusions can be drawn about the loss of polarization phenomenon that we introduce in this paper.

APPENDIX E: ADDITIONAL PLOTS FOR DIFFERENT MATERIALS

Here we present data obtained by performing experiments in glass, liquid water, and high-pressure nitrogen gas (23 bar) in the normal-GVD regime. In each figure (Figs. 6, 7, and 8), the left two subplots show results for linearly polarized input, and the right two subplots show results for elliptically polarized input. We used 800-nm, 50-fs pulses at a 10-Hz repetition rate at different input energies (below and above the collapse threshold in each case). In the experiment, we compare output s/p ratio fluctuations for elliptically polarized input and linearly polarized input for fixed fluctuations (10%) in input energy. These fluctuations in the s/p ratio directly correspond to fluctuations in output polarization angle θ.

[1] G. Fibich and G. Papanicolaou, SIAM J Appl. Math. **60**, 183 (1999).
[2] G. Fibich and A. L. Gaeta, Opt. Lett. **25**, 335 (2000).
[3] A. L. Gaeta, Phys. Rev. Lett. **84**, 3582 (2000).
[4] R. W. Boyd, S. G. Lukishova, and Y. R. Shen, *Self-Focusing: Past and Present: Fundamentals and Prospects* (Springer Science & Business Media, New York, 2008).
[5] G. Fibich, *The Nonlinear Schrödinger Equation: Self-Focusing and Optical Collapse* (Springer, New York, 2015).

[6] A. Couairon and A. Mysyrowicz, Phys. Rep. **441**, 47 (2007).
[7] V. P. Kandidov, S. A. Shlenov, and O. G. Kosareva, Quantum Electron. **39**, 205 (2009).
[8] B. Shim, S. E. Schrauth, and A. L. Gaeta, Opt. Exp. **19**, 9118 (2011).
[9] M. Rodriguez, R. Bourayou, G. Méjean, J. Kasparian, J. Yu, E. Salmon, A. Scholz, B. Stecklum, J. Eislöffel, U. Laux, A. P. Hatzes, R. Sauerbrey, L. Wöste, and J.-P. Wolf, Phys. Rev. E **69**, 036607 (2004).
[10] J. Kasparian, M. Rodriguez, G. Méjean, J. Yu, E. Salmon, H. Wille, R. Bourayou, S. Frey, Y.-B. André, A. Mysyrowicz, R. Sauerbrey, J.-P. Wolf, and L. Wöste, Science **301**, 61 (2003).
[11] J. Kasparian and J.-P. Wolf, Opt. Exp. **16**, 466 (2008).
[12] C. P. Hauri, W. Kornelis, F. W. Helbing, A. Heinrich, A. Couairon, A. Mysyrowicz, J. Biegert, and U. Keller, Appl. Phys. B **79**, 673 (2004).
[13] M. Negro, C. Vozzi, F. Calegari, S. D. Silvestri, and S. Stagira, *CLEO/Europe and EQEC 2011 Conference Digest* (Optical Society of America, Munich, Germany, 2011), p. CF7_3.
[14] M. Negro, C. Vozzi, F. Calegari, S. D. Silvestri, and S. Stagira, Opt. Lett. **35**, 1350 (2010).
[15] T. Popmintchev, M.-C. Chen, D. Popmintchev, P. Arpin, S. Brown, S. Ališauskas, G. Andriukaitis, T. Balčiunas, O. D. Mücke, A. Pugzlys, A. Baltuska, B. Shim, S. E. Schrauth, A. L. Gaeta, C. Hernández-García, L. Plaja, A. Becker, A. Jaron-Becker, M. M. Murnane, and H. C. Kapteyn, Science **336**, 1287 (2012).
[16] T. I. Oh, Y. S. You, N. Jhajj, E. W. Rosenthal, H. M. Milchberg, and K. Y. Kim, New J. Phys. **15**, 075002 (2013).
[17] P. A. Robinson, Rev. Mod. Phys. **69**, 507 (1997).
[18] Y. S. Kivshar and D. E. Pelinovsky, Phys. Rep. **331**, 117 (2000).
[19] L. P. Pitaevskii, Phys. Lett. A **221**, 14 (1996).
[20] S. K. Turitsyn, Phys. Rev. E **47**, R13(R) (1993).
[21] F. Merle, Commun. Pure Appl. Math. **45**, 203 (1992).
[22] G. Fibich and M. Klein, Nonlinearity **24**, 2003 (2011).
[23] B. Shim, S. E. Schrauth, A. L. Gaeta, M. Klein, and G. Fibich, Phys. Rev. Lett. **108**, 043902 (2012).
[24] A. Sagiv, A. Ditkowski, and G. Fibich, Opt. Expr. **25**, 24387 (2017).
[25] M. Mlejnek, M. Kolesik, J. V. Moloney, and E. M. Wright, Phys. Rev. Lett. **83**, 2938 (1999).
[26] L. Bergé, S. Skupin, F. Lederer, G. Méjean, J. Yu, J. Kasparian, E. Salmon, J. P. Wolf, M. Rodriguez, L. Wöste, R. Bourayou, and R. Sauerbrey, Phys. Rev. Lett. **92**, 225002 (2004).
[27] S. Varma, Y.-H. Chen, and H. M. Milchberg, Phys. Rev. Lett. **101**, 205001 (2008).
[28] G. Fibich, S. Eisenmann, B. Ilan, and A. Zigler, Opt. Lett. **29**, 1772 (2004).
[29] Z.-Q. Hao, J. Zhang, T.-T. Xi, X.-H. Yuan, Z.-Y. Zheng, X. Lu, M.-Y. Yu, Y.-T. Li, Z.-H. Wang, W. Zhao, and Z.-Y. Wei, Opt. Exp. **15**, 16102 (2007).
[30] G. Point, Y. Brelet, A. Houard, V. Jukna, C. Milián, J. Carbonnel, Y. Liu, A. Couairon, and A. Mysyrowicz, Phys. Rev. Lett. **112**, 223902 (2014).
[31] Y. Shi, A. Chen, Y. Jiang, S. Li, and M. Jin, Opt. Commun. **367**, 174 (2016).
[32] N. A. Panov, V. A. Makarov, V. Y. Fedorov, and O. G. Kosareva, Opt. Lett. **38**, 537 (2013).
[33] L. Bergé, C. Gouédard, J. Schjødt-Eriksen, and H. Ward, Physica D **176**, 181 (2003).
[34] G. Fibich and B. Ilan, Opt. Lett. **26**, 840 (2001).
[35] G. Fibich and B. Ilan, Physica D **157**, 112 (2001).
[36] G. Fibich and B. Ilan, Phys. Rev. Lett. **89**, 013901 (2002).
[37] G. Fibich and B. Ilan, Phys. Rev. E **67**, 036622 (2003).
[38] Y. S. You, T. I. Oh, and K.-Y. Kim, Opt. Lett. **38**, 1034 (2013).
[39] A. K. Dharmadhikari, S. Edward, J. A. Dharmadhikari, and D. Mathur, J. Phys. B **48**, 094012 (2015).
[40] S. Rostami, M. Chini, K. Lim, J. P. Palastro, M. Durand, J.-C. Diels, L. Arissian, M. Baudelet, and M. Richardson, Sci. Rep. **6**, 20363 (2016).
[41] M. Kolesik, J. V. Moloney, and E. M. Wright, Phys. Rev. E **64**, 046607 (2001).
[42] N. Phuxuan, J. L. Ferrier, J. Gazengel, and G. Rivoire, Opt. Commun. **46**, 329 (1983).
[43] S. Petit, A. Talebpour, A. Proulx, and S. L. Chin, Opt. Commun. **175**, 323 (2000).
[44] S. Yuan, T.-J. Wang, H. Pan, L. Zheng, S. L. Chin, and H. Zeng, Opt. Exp. **23**, 5582 (2015).
[45] S. Yuan, T.-J. Wang, O. Kosareva, N. Panov, V. Makarov, H. Zeng, and S. L. Chin, Phys. Rev. A **84**, 013838 (2011).
[46] O. Kosareva, N. Panov, V. Makarov, I. Perezhogin, C. Marceau, Y. Chen, S. Yuan, T. Wang, H. Zeng, A. Savel'ev, and S. L. Chin, Opt. Lett. **35**, 2904 (2010).
[47] S. Rostami, J.-C. Diels, and L. Arissian, Opt. Exp. **23**, 3299 (2015).
[48] A. H. Sheinfux, E. Schleifer, J. Papeer, G. Fibich, B. Ilan, and A. Zigler, Appl. Phys. Lett. **101**, 201105 (2012).
[49] G. P. Agrawal, *Nonlinear Fiber Optics*, 5th ed. (Elsevier/Academic Press, Amsterdam, 2013).
[50] A. Ditkowski, G. Fibich, and A. Sagiv, arXiv:1803.10991 [physics] (2018).
[51] E. Hecht, *Optics*. 3rd ed. (Addison-Wesley, 1998), p. 322.
[52] A. Brodeur and S. L. Chin, Phys. Rev. Lett. **80**, 4406 (1998).
[53] A. Brodeur and S. L. Chin, J. Opt. Soc. Am. B **16**, 637 (1999).
[54] Y. Yang, M. Liao, X. Li, W. Bi, Y. Ohishi, T. Cheng, Y. Fang, G. Zhao, and W. Gao, J. Appl. Phys. **121**, 023107 (2017).
[55] R. W. Boyd, *Nonlinear Optics*, 3rd ed. (Academic Press, Orlando, FL, 2008), pp. 217–221.
[56] K. D. Moll and A. L. Gaeta, Opt. Lett. **29**, 995 (2004).
[57] L. Bergé and S. Skupin, Phys. Rev. E **71**, 065601 (2005).
[58] S. Skupin and L. Bergé, Physica D **220**, 14 (2006).
[59] M. Durand, A. Jarnac, A. Houard, Y. Liu, S. Grabielle, N. Forget, A. Durécu, A. Couairon, and A. Mysyrowicz, Phys. Rev. Lett. **110**, 115003 (2013).
[60] R.-P. Chen, K.-H. Chew, and S. He, Sci. Rep. **3**, 1406 (2013).
[61] R.-P. Chen, L.-X. Zhong, K.-H. Chew, T.-Y. Zhao, and X. Zhang, Laser Phys. **25**, 075401 (2015).
[62] S.-M. Li, Y. Li, X.-L. Wang, L.-J. Kong, K. Lou, C. Tu, Y. Tian, and H.-T. Wang, Sci. Rep. **2**, 1007 (2012).
[63] S.-M. Li, Z.-C. Ren, L.-J. Kong, S.-X. Qian, C. Tu, Y. Li, and H.-T. Wang, Photonics Res. **4**, B29 (2016).